

## Article

# Electrochemical Performance and Conductivity of N-Doped Carbon Nanotubes Annealed under Various Temperatures as Cathode for Lithium-Ion Batteries

Zhengjun Zhong<sup>1</sup> , Soroosh Mahmoodi<sup>2</sup>, Dong Li<sup>1</sup> and Shengwen Zhong<sup>1,\*</sup>

<sup>1</sup> Jiangxi Key Laboratory of Power Battery and Materials, Department of Materials Metallurgy Chemistry, Jiangxi University of Science and Technology, Ganzhou 341000, China

<sup>2</sup> School of Information Engineering, Yancheng Teachers University, Yancheng 224000, China

\* Correspondence: zhongsw-jxust@outlook.com; Tel.: +86-13979707564

**Abstract:** Nitrogen-doped carbon nanotubes (NCNTs) are obtained using a post-treatment method under different sintering temperatures. The catalysts can be removed from the Carbon Nanotubes (CNTs) within an acid treatment process. Then, the purified CNTs can be employed as a nitrogen doping basis. This research adds melamine as a nitrogen source during the sintering procedure under different temperatures to achieve NCNTs, which are applied to the cathodes. LiMn<sub>2</sub>O<sub>4</sub> (LMO) cathode slurries are prepared using pristine CNTs and NCNTs samples as conductive additives. Coin cell lithium-ion batteries (LIBs) are fabricated using slurry samples. X-ray photoelectron spectroscopical analysis shows the nitrogen doping degree is up to 5 atom%, and graphitic-N nitrogen groups are the dominating species present on the NCNT's surface while being treated at 800 °C. Graphitic-N nitrogen groups improve the conductivity and surface area of the NCNTs, which increases the rate capacity (106.8 mA h g<sup>-1</sup> at 5 C) and cyclic retention (92.45% of initial capacity after 200 cycles at 5 C) of the lithium-ion batteries. The morphology of the NCNTs, the concentration of NCNTs elements, and the electrochemical performances of coin cell batteries are extensively discussed.

**Keywords:** nitrogen-doped; carbon nanotubes; melamine; graphitic-N nitrogen groups; lithium-ion batteries



**Citation:** Zhong, Z.; Mahmoodi, S.; Li, D.; Zhong, S. Electrochemical Performance and Conductivity of N-Doped Carbon Nanotubes Annealed under Various Temperatures as Cathode for Lithium-Ion Batteries. *Metals* **2022**, *12*, 2166. <https://doi.org/10.3390/met12122166>

Academic Editor: José Valdemar Fernandes

Received: 8 October 2022

Accepted: 9 December 2022

Published: 16 December 2022

**Publisher's Note:** MDPI stays neutral with regard to jurisdictional claims in published maps and institutional affiliations.



**Copyright:** © 2022 by the authors. Licensee MDPI, Basel, Switzerland. This article is an open access article distributed under the terms and conditions of the Creative Commons Attribution (CC BY) license (<https://creativecommons.org/licenses/by/4.0/>).

## 1. Introduction

Lithium-ion batteries (LIBs) benefit from high energy density, long cycle life, and abundant raw material reserves. LIBs are new energy storage sources that have been gradually applied on a large scale. The LIBs have gained the attention of various industries, especially for electrical vehicle applications [1,2]. LIBs consist of several parts, while the cathode plays a vital role in the efficiency of lithium-ion batteries.

The cathode materials are semiconductors that cannot rely on their conductivity for adequate electron transportation without chemical treatments. Adding nano-scale carbon materials enhances the conductivity of cathode materials under specific situations [3].

The unique one-dimensional morphology of carbon nanotubes is more effective than the conductive carbon black and graphite in forming conductive electronic networks [4,5]. The high specific surface area (SSA) of carbon nanotubes creates a stronger electrolyte adsorption ability, which increases the electrolyte infiltration and thus improves the Li-ion transfer rate [6]. Chemical vapor deposition (CVD) has recently been a well-known method for producing large-scale commercial carbon nanotubes. Acid treatment is generally used to remove catalysts particles such as iron, cobalt, and nickel to purify carbon nanotubes. It leads to lattice defects of carbon nanotubes and forming oxygen functional groups on their surface. However, acid treatment reduces the conductivity of carbon nanotubes. Meanwhile, carbon nanotubes' lattice defects and oxygen functional groups as the active basis are proper for heteroatom doping such as nitrogen, phosphorus, sulfur, and boron [7–10]. Nitrogen and

carbon have a similar atomic radius. Therefore, incorporating nitrogen atoms into the carbon matrix to form a nitrogen-binding configuration would not lead to a significant lattice mismatch [11]. The N binding configuration enhances the hydrophilicity of the NCNTs' sidewalls and increases the dispersion of NCNTs in solvents [12]. In particular, the nitrogen atoms doped in the graphite matrix act as electron donors to promote n-type conductivity and improve the carbon nanotubes' electron transport ability [13–16]. Carbon nanotubes with greater conductivity and one-dimensional structure satisfy the industrial demands for the fast charging of lithium-ion batteries. Direct growth and post-synthesis methods have been commonly employed in preparing NCNTs [17]. Direct growth is a method to simultaneously pyrolysis the carbon and nitrogen sources on the catalyst for synthesizing NCNTs. The post-synthesis is a method to mix and anneal the CNTs prepared from the nitrogen sources such as TPT, cyanamide, urea, and ammonia [15,18–20]. Melamine also contains high nitrogen sources while not being saturated by C–N bonds. Therefore, melamine in a post-synthesis method results in higher nitrogen doping amounts [21,22].

Several researchers focused on applying NCNTs for the negative electrodes (anode) and catalyst carriers [17,23,24]. However, the application of NCNTs as conductive additives for fabricating the cathode electrode has never been intensely investigated. This research investigates an efficient synthesis of N-doped carbon nanotubes via a thermal reaction between carbon nanotubes and melamine. It is proposed that the NCNTs, as the conductive networks, increase the proportion of a cathode material's free electrons to improve the performances of lithium-ion batteries. In this experimental study, NCNTs and cathode material are stirred into a homogenous slurry to construct efficient conductive networks. The N binding configurations of NCNTs are characterized by an X-ray photoelectron spectroscopy (XPS) device. Furthermore, the morphology and microstructure of the NCNTs are imaged and characterized by the SEM, TEM, and BET apparatuses. Finally, the electrochemical performances of fabricated batteries are evaluated to confirm the reliability of the mentioned propositions.

## 2. Materials and Methods

### 2.1. Preparation of CNTs

The Fe–Al catalyst was prepared by an impregnation method. It was used to prepare multi-walled carbon nanotubes (CNTs) by chemical vapor deposition (CVD). A ferric nitrate solution was mixed with an alumina nano-powder. Firstly, the mixture was frozen at  $-40\text{ }^{\circ}\text{C}$  in a vacuum chamber to obtain a dry catalyst precursor, and then it was calcined at  $800\text{ }^{\circ}\text{C}$  to obtain the catalyst powder. The catalyst powder was annealed in an argon tube furnace of  $680\text{ }^{\circ}\text{C}$ . Iron monomers are formed in the catalyst under the effect of hydrogen reduction. Subsequently, propane as a carbon source was blown into the furnace [25]. After decomposition, the propane is dissolved into the iron monomers and then saturated and precipitated, gradually generating the CNTs [26]. The CNTs with aqua regia ( $\text{HCl}/\text{HNO}_3 = 3:1$ ) were incubated in an oil bath of  $90\text{ }^{\circ}\text{C}$  for 6 h to remove the catalyst within the purification process. The CNTs were washed with deionized water of 7.0 pH. Finally, it was filtered to obtain the purified CNTs, as the first sample of this experiment. The details of CNTs sample preparation are shown in Table 1.

**Table 1.** Details of CNTs and NCNTs samples preparation.

Sample	Annealing Temperature	Annealing Times	Polyacrylic Acid Existence	NCNTs or CNTs Concentrations (wt%)	LMO+PVDF Concentrations (wt%)
CNT	Room temperature	N/A	none	2%	95% + 3%
NCNT-700	700 °C	2 h	contain	2%	95% + 3%
NCNT-800	800 °C	2 h	contain	2%	95% + 3%
NCNT-900	900 °C	2 h	contain	2%	95% + 3%
NCNT-1000	1000 °C	2 h	contain	2%	95% + 3%

## 2.2. Preparation of NCNTs

The purified CNTs were mixed with melamine in a mass ratio of 1:1. The mixed powder was grounded to obtain a uniform mixture. The polyacrylic acid aqueous solution was added to the prepared mixture and stirred to apply carboxyl groups on the surface of CNTs. The amine group in melamine has a strong hydrogen bonding ability, which allows melamine to be adsorbed on the surface of CNTs [27]. The suspension dried at 70 °C for 24 h to obtain grey chunk pieces. The grey chunks were grounded into a powder and then sintered at 700–1000 °C for 2 h under argon gas. During the decomposition of melamine and carboxyl groups, nitrogen enters into the defects of CNTs to obtain the N-doped carbon nanotubes (NCNTs). Four samples of the sintered NCNTs under different temperatures are prepared. The details of the samples' preparation are shown in Table 1.

## 2.3. Preparation of Batteries

The purified CNTs and NCNTs samples were dispersed in an N-methyl-2-pyrrolidone (NMP) solution by ultrasound and ball milling methods to obtain a uniformly dispersed conductive slurry. In this research, commercial LiMn<sub>2</sub>O<sub>4</sub>(LMO) and polyvinylidene fluoride (PVDF) were purchased as the cathode materials and binder, respectively. The concentrations of coating elements are shown in Table 1. Five sets of cathodes using the slurries with different conductive additives (CNTs and NCNTs samples) were coated on the surface of an aluminum foil. The coated cathode electrodes were then dried in an air furnace of 120 °C for an hour.

Lithium metal foils, Celgard 2400, and LiPF<sub>6</sub>/EC+DMC+EMC (volume ratio of 1:1:1) were purchased as the battery anode, separator, and electrolyte, respectively. Five sets of CR2032 coin cells were assembled using the fabricated cathode electrodes by applying 1.0 mol/L of electrolyte.

# 3. Results and Discussion

## 3.1. Morphology of N-Doped Carbon Nanotubes by EDS

The surface morphology, microstructure, and elemental distribution of samples are imaged and measured by a Scanning Electron Microscope (SEM, JSM7800F) apparatus and Energy Dispersive Spectroscopy (EDS) method. Figure 1a–d shows the surface SEM images of NCNTs samples (displayed on the left side of Figure 1) and the EDS measurements (in the middle and right side of Figure 1). Some literature represents that the melamine can be decomposed entirely at annealing temperatures higher than 350 °C under argon gas treatment and would not remain like any other organic substances [28,29]. Therefore, if the melamine cannot completely be decomposed, it might appear in the form of other organic substances containing nitrogen. Consequently, it is impossible to determine whether the nitrogen element sources are mainly released from the NCNTs. It is hypothesized that most of the N elements shown in EDS images might come from NCNT sources. Therefore, the XPS measurements are performed and discussed in the next section (Section 3.2) to approve the above-mentioned hypothesis.

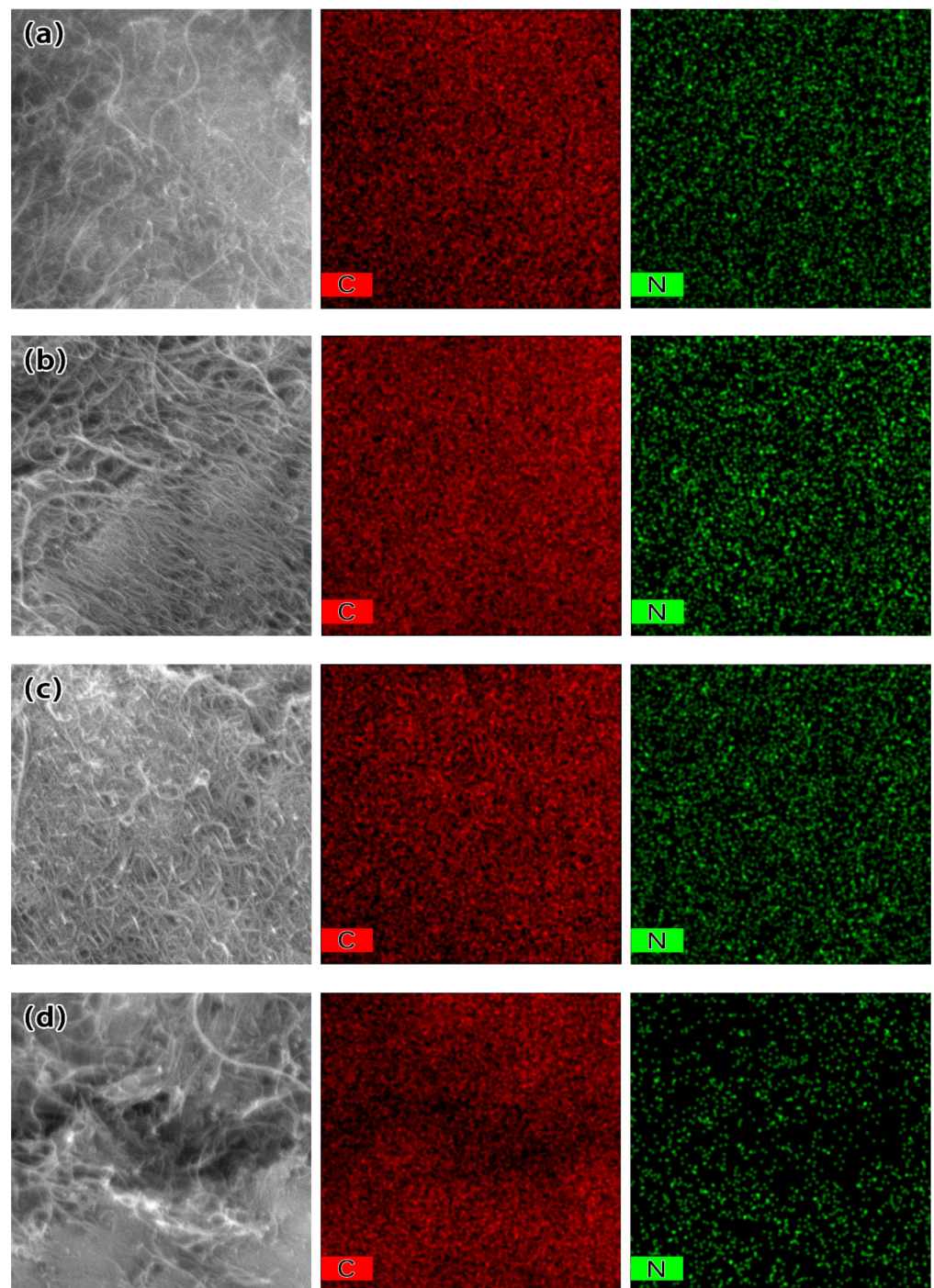


**Figure 1.** (a–d): SEM characterization (left side) and EDS measurements of the samples (a) NCNT-700, (b) NCNT-800, (c) NCNT-900, and (d) NCNT-1000 (middle and right side).

### 3.2. Characterization of N-Doped Carbon Nanotubes

N1s peaks can be further deconvoluted into three different peaks at the binding energies of  $(398 \pm 0.5 \text{ eV})$ ,  $(400 \pm 0.5 \text{ eV})$ , and  $(401.3 \pm 0.5 \text{ eV})$ , corresponding to pyridinic-N, pyrrolic-N, and graphitic-N species, respectively [30–32]. The pyridinic-N species is an  $sp^2$  hybridized N atom with two  $sp^2$  hybridized C neighbors. The pyrrolic-N atoms break the honeycomb structures and change them into five-membered rings [33]. The pyridinic-N and the pyrrolic-N can become highly active doping sites for other heteroatoms or active sites for catalysis [10]. The graphitic-N species represents that N atoms are replaced instead of one C atom inside the graphite matrix and would be bonded with three C ( $sp^2$

hybridized) atoms. For a better understanding, a schematic is drawn in Figure 2, which shows the carbon nanotubes, graphite matrix, and bonding interactions. After applying excessive  $\pi$ -electrons into the graphitic plane, the density of the n-type carrier is increased and enhances carbon nanotubes' conductivity [17].

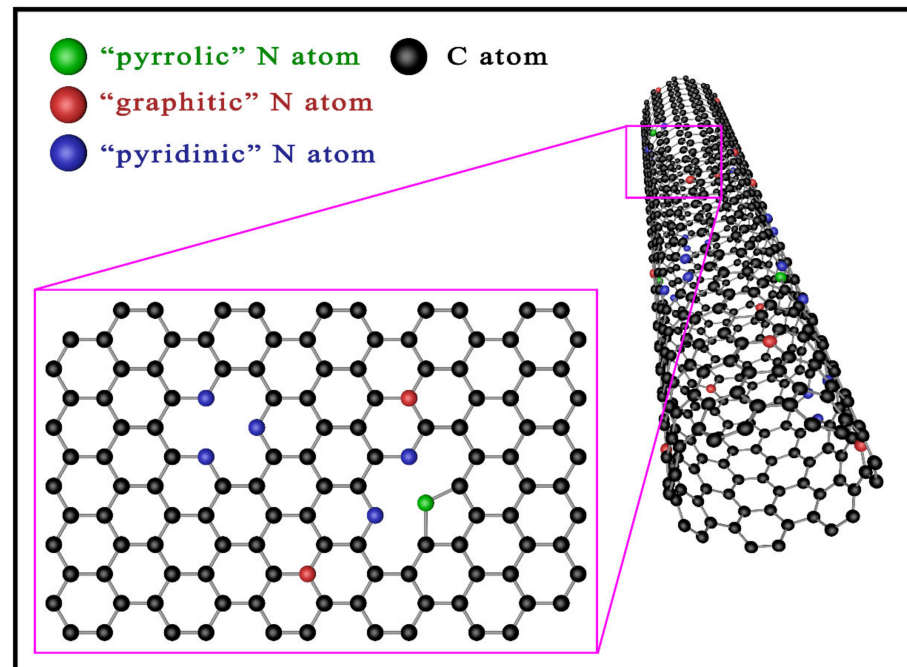


Figure 2. A schematic of carbon nanotubes, graphite matrix, and bonding interactions.

The samples' bonding configuration and doping concentration are characterized by an X-ray photoelectron spectroscopy (XPS, Thermo Scientific K-Alpha+). Figure 3a shows that the predominant peaks around 284 eV, 402 eV, and 532 eV correspond to the characteristic peaks of C1s, N1s, and O1s, respectively. The bond structures of the nitrogen atoms incorporated in NCNTs samples were analyzed by XPS using the high-resolution peaks of N1s ranging from 394 to 407 eV. Figure 3b–f shows the high-resolution peaks of CNTs, NCNT-700, NCNT-800, NCNT-900, and NCNT-1000 samples, respectively.

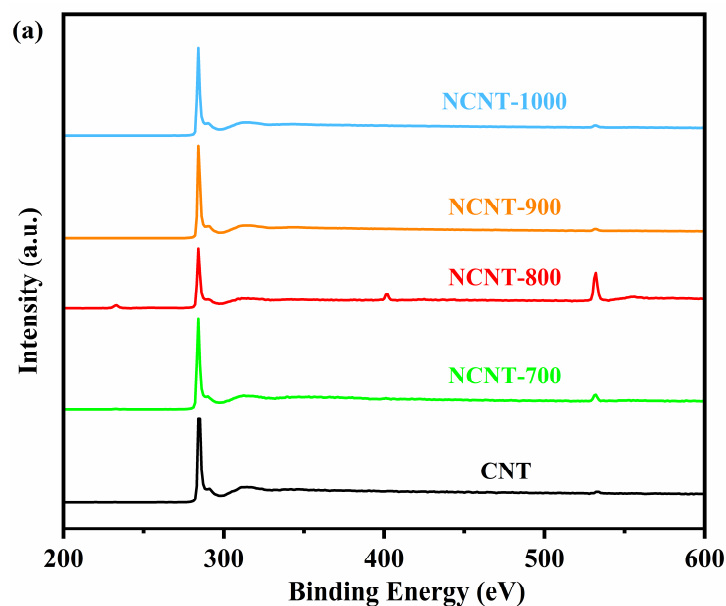


Figure 3. Cont.

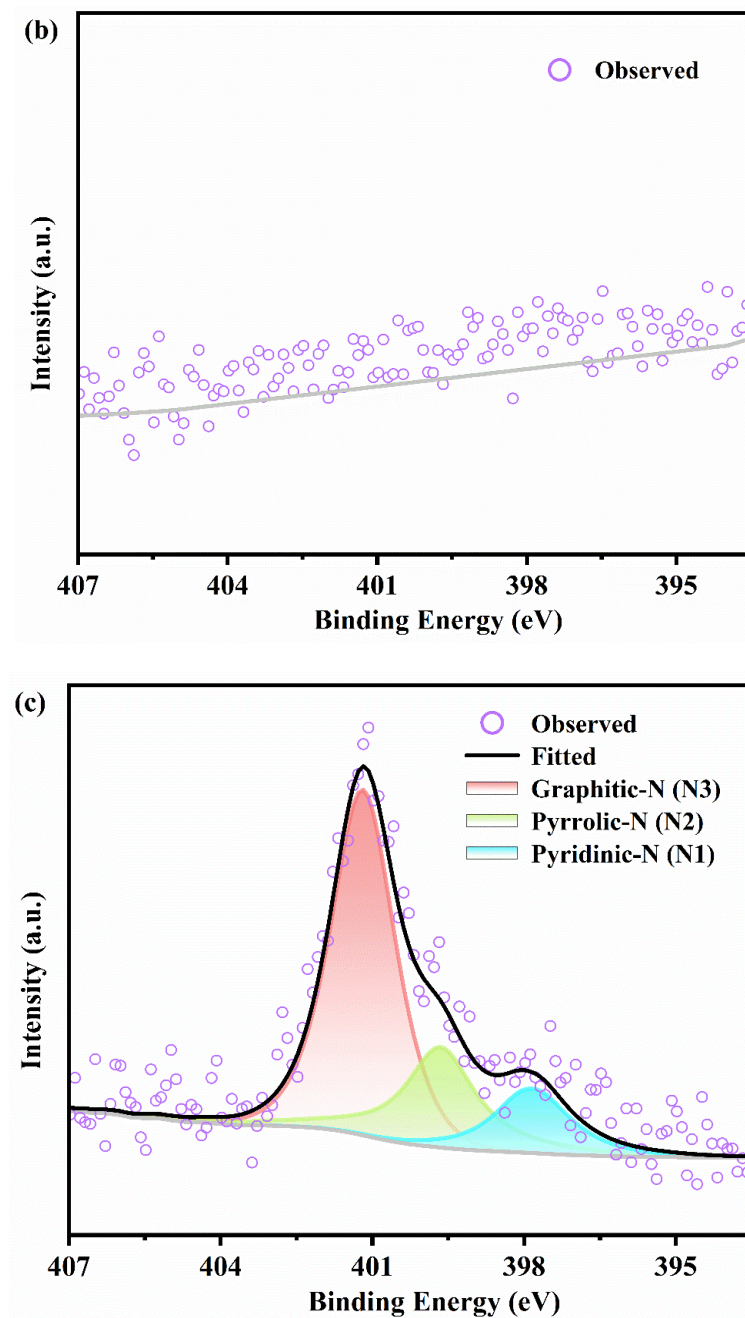


Figure 3. Cont.

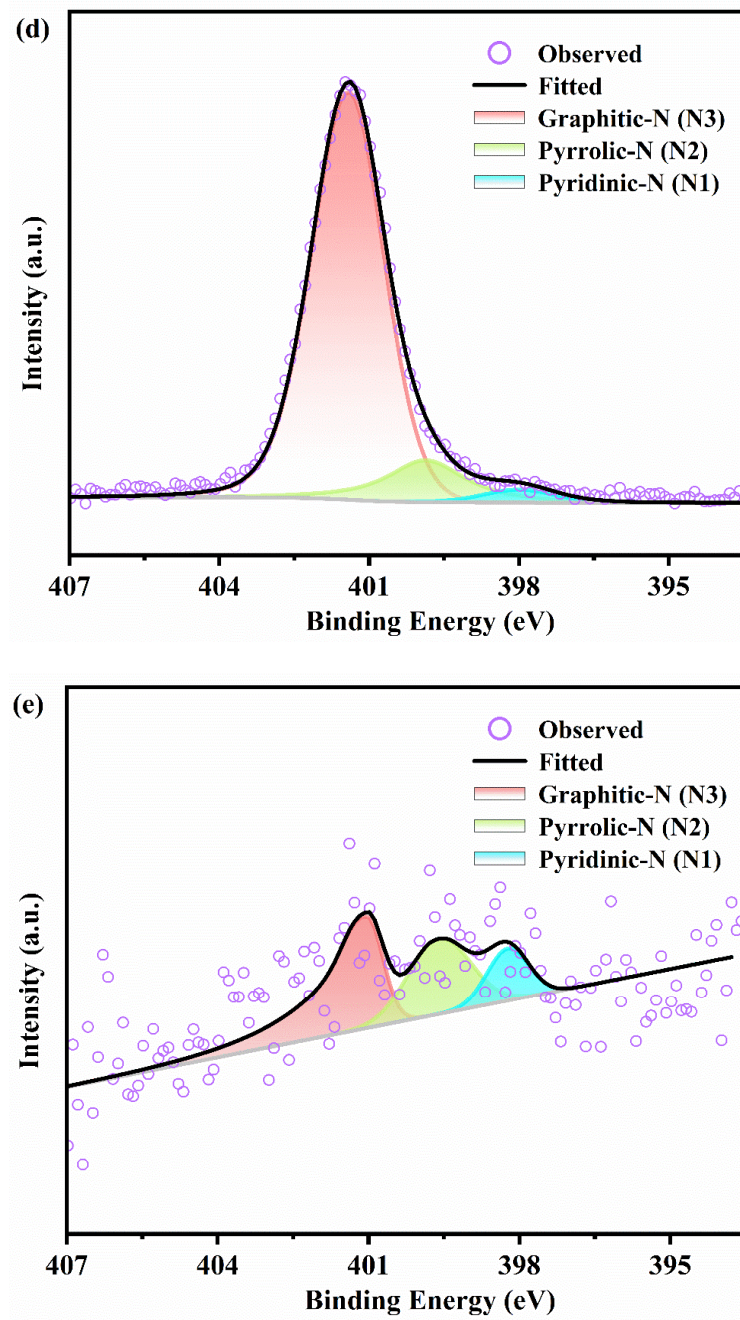
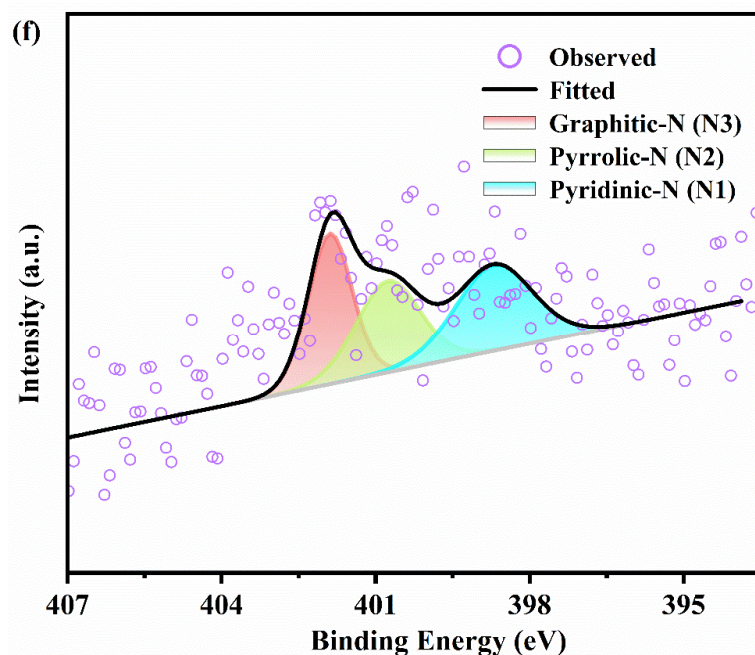


Figure 3. Cont.



**Figure 3.** (a–f): (a) X-ray photoelectron spectroscopy of samples. XPS survey of N1s patterns of samples (b) CNT, (c) of NCNT-700, (d) NCNT-800, (e) NCNT-900, and (f) NCNT-1000.

The total amount of N doping content and different N binding configuration proportion for each sample is measured by XPS and numerically evaluated by Avantage software, which is represented in Table 2. The NCNT-800 sample shows the highest N doping content of 5.55 atom%, and the proportion of its graphitic-N species was evaluated at 88.16%. A comparison between the XPS results of all annealed samples under different temperatures showed that the most elevated nitrogen was obtained in the NCNTs sample annealed at 800 °C. Therefore, it concluded that the types and ratios of nitrogen species are sensitive to the annealing temperature.

Pyridinic-N and pyrrolic-N are converted to a more thermally stable graphitic-N species at higher temperatures. Thus, doping N into the graphite matrix might form graphitic-N species that require overcoming a higher energy barrier [21,34]. In this study, the N1s peak intensities and areas of NCNT-900 and NCNT-1000 samples decreased significantly, indicating that the N doping content was reduced. This phenomenon was discussed as the effects of post-synthesis and direct growth methods [35–37]. Researchers believe that a decrease in the N doping content might happen due to the breakage of the C–N bond at higher temperatures, which leads to the removal of the N element [36,38,39]. In this study, we hypothesize that the decrease in the N doping content might be due to the decomposition products of melamine inside a tube furnace under the flow of argon gas before achieving sufficient nitrogen doping.

Generally, there are two main effects of adding polyacrylic acid as the hydrogels. First, it assists in mixing carbon nanotubes with melamine more uniformly. Second, polyacrylic acid hydrogels contain a large number of hydrophilic carboxyl groups, while the decomposition of carboxyl groups provides active sites during a thermal treatment [22]. We hypothesize that adding polyacrylic acid to the mixture of carbon nanotubes and melamine might induce more N atoms to be doped into the graphite matrix. Therefore, besides this study, two samples of NCNTs treated under 800 °C with and without adding the polyacrylic acid were also prepared and tested to approve this proposition. The XPS measurements evaluate the ratio of N atoms that increased from 2.94% to 5.55% for the NCNTs sample that contains the polyacrylic acid hydrogels (shown in Figure 4).

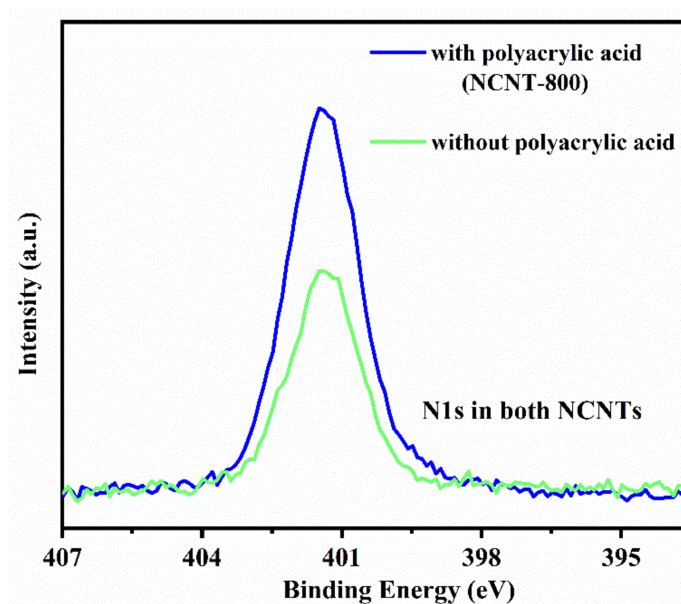


**Figure 4.** The percentage of N atoms for both samples of NCNTs treated under 800 °C with and without adding the polyacrylic acid evaluated by The XPS measurements.

The Specific Surface Area (SSA) can be evaluated by the Brunauer–Emmett–Teller (BET) method. A higher SSA improves the contact interface between NCNTs and electrolytes, enhancing the ion batteries' performance. The SSA of all NCNTs samples is measured by a BET (BeiShiDe 3H-2000 PM1) instrument. Figure S1 presents samples' N<sub>2</sub> adsorption/desorption isotherms, summarized in Table 2. The SSA of the purified carbon nanotubes (CNTs) sample was evaluated at 210.2 m<sup>2</sup> g<sup>−1</sup>, whereas other NCNTs samples showed a higher value. The BET results showed that the highest value was evaluated at 238.32 m<sup>2</sup> g<sup>−1</sup> for the NCNT-800 sample.

**Table 2.** Types and contents of nitrogen binding configuration.

Sample	SSA (m <sup>2</sup> g <sup>−1</sup> )	N Content (Atom.%)	Area Composition of Different N(%) Structures Sorted by Peak Positions		
			Pyridinic-N	Pyrrolic-N	Graphitic-N
NCNT-700	220.95	1.14	13.06	36.02	50.92
NCNT-800	238.32	5.55	2.81	9.03	88.16
NCNT-900	236.62	0.47	15.28	32.74	51.98
NCNT-1000	231.65	0.23	44.54	31.77	23.68
CNT	210.21	-	-	-	-

Figure 5a,b show the morphology of the carbon nanotube (NCNT-800 sample) captured by Scanning Electron Microscopy (SEM, JSM7800F) and by Transmission Electron Microscopy (TEM, JEOL JEM-2100), respectively. The observed TEM morphology of NCNT-800 in this study is similar to that of NCNT prepared by a post-synthesis method in the literature of another work [10] and not similar to the TEM observation of that the NCNT prepared by a direct growth method [23,40]. An SEM image of the electrode using NCNT-800 is shown in Figure 5c. The SEM image shows that the NCNT-800 is uniformly distributed on the surface of each cathode active material and forms a continuous conductive network.

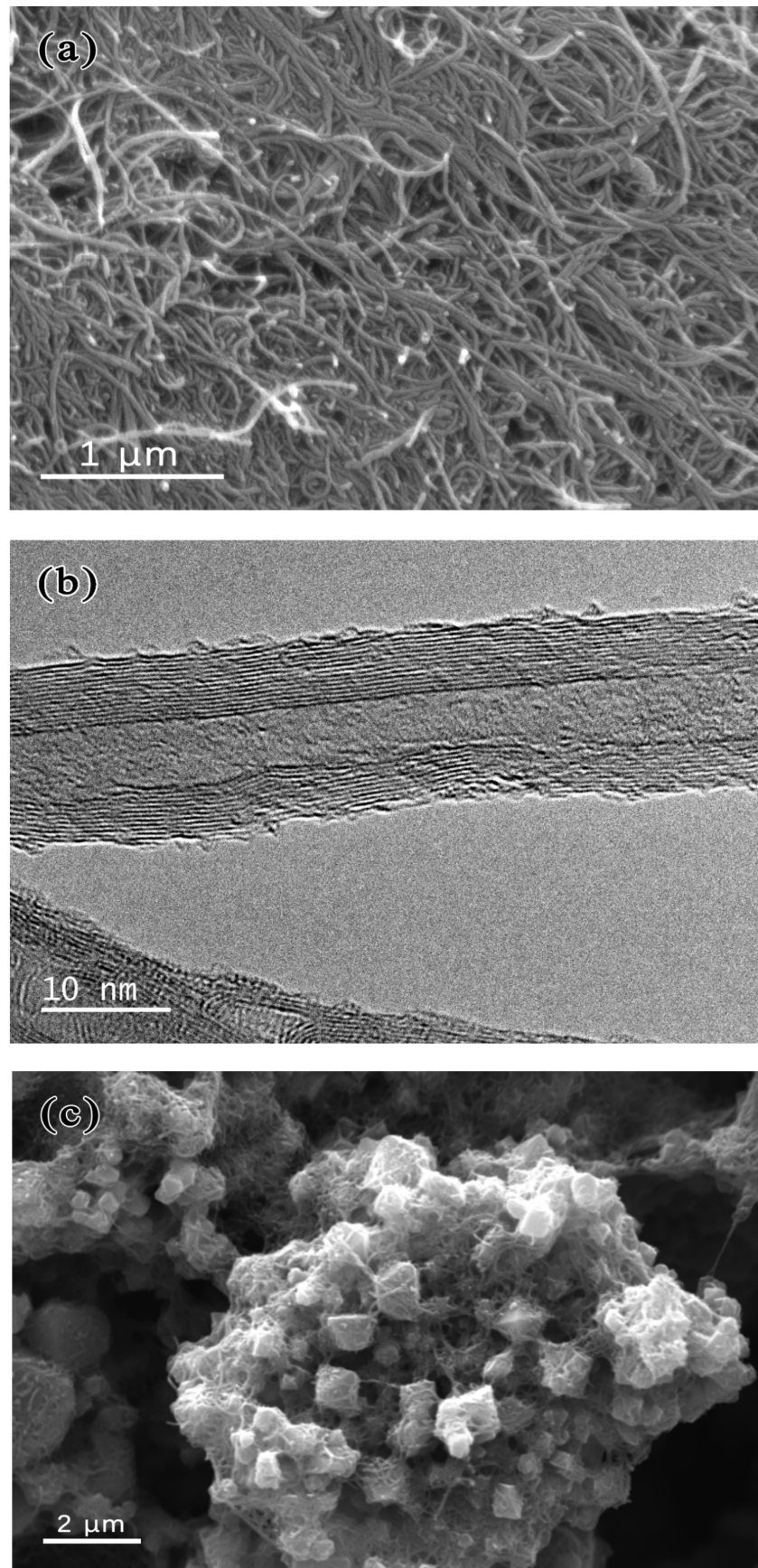


**Figure 5.** Morphology of NCNT-800 sample captured by SEM (a), TEM (b), and SEM image of B-NCNT-800 electrode (c).

### 3.3. Evaluation of Electrochemical Performance

#### 3.3.1. Conductivity and Resistivity Measurements

The cathode slurries of CNTs and NCNTs samples were coated on an insulating substrate and dried at 120 °C for half an hour to prepare five coated films. The coated films using the CNTs and NCNTs slurries are labeled as S-CNT, S-NCNT-700, S-NCNT-800, S-NCNT-900, and S-NCNT-1000. The electrical conductivity and resistivity of the prepared cathodes were measured by a four-point conductive probe (RTS-9). Figure 6 shows the measured conductivity and resistance of cathode samples. Table 3 shows the values of average conductivity and resistivity for all prepared cathodes.

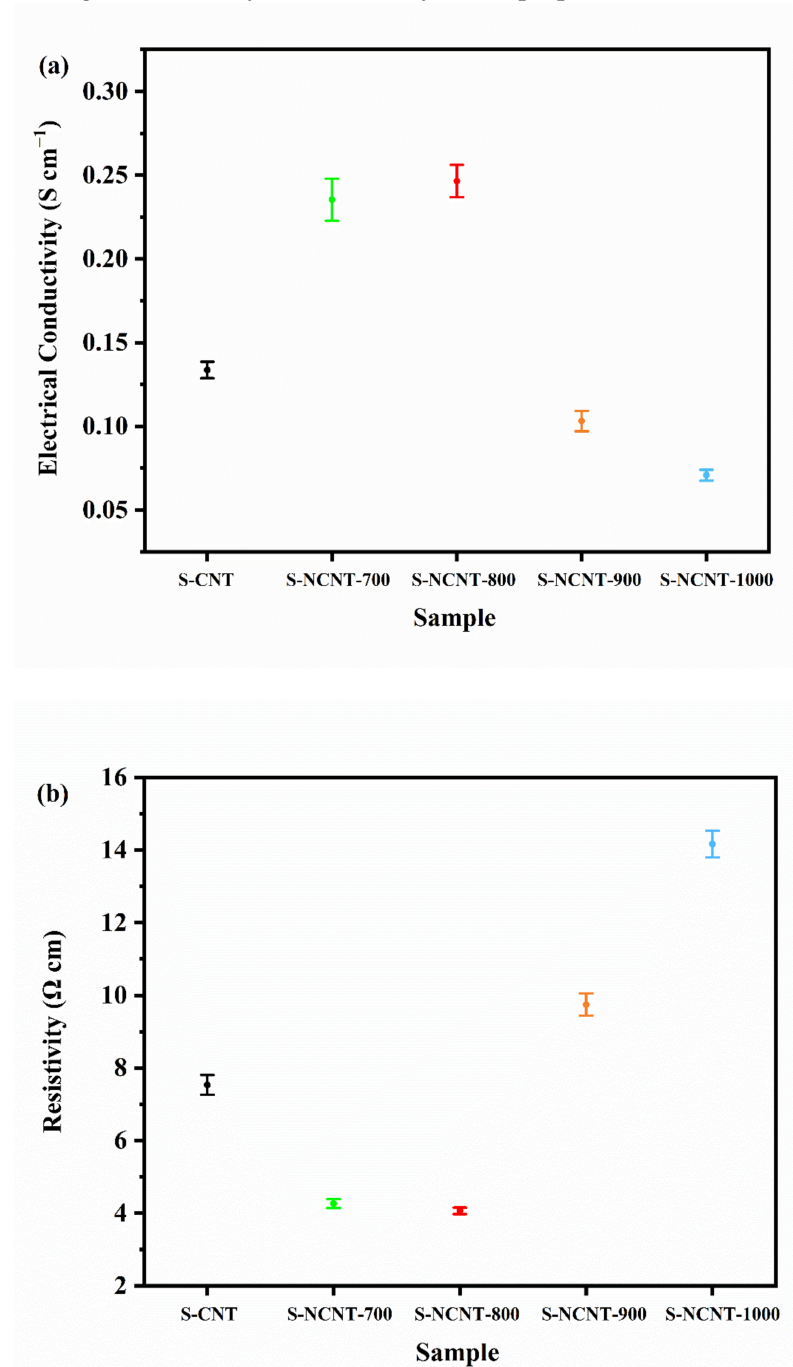


Figure 6. (a) Electrical conductivity and (b) resistivity of cathodes coated on insulating films.

**Table 3.** Average electrical conductivity and resistivity of samples.

Sample	S-CNT	S-NCNT-700	S-NCNT-800	S-NCNT-900	S-NCNT-1000
Conductivity (S cm <sup>-1</sup> )	0.133	0.235	0.246	0.103	0.071
Resistivity (Ω cm)	7.533	4.267	4.067	9.744	14.167

The measurements by the RTS-9 device resulted in the highest slurry conductivity valued at 0.246 S cm<sup>-1</sup> belonging to the S-NCNT-800 sample, whereas the lowest one belonged to the S-NCNT-1000. S-NCNT-700 and S-NCNT-800 samples showed higher conductivity than the pristine carbon nanotubes (S-CNT) samples, whereas the S-NCNT-900 and S-NCNT-1000 revealed a lower one. There might be two reasons for the decrease in conductivity. First, S-NCNT-900 and S-NCNT-1000 samples fail to dope nitrogen atoms into the graphite matrix of the carbon nanotube. Second, although high-temperature treatment can remove most oxygen functional groups to improve electrical conductivity [41,42], the conglutination of carbon-based materials during a high-temperature treatment might be inevitable [15]. Therefore, forming a continuous conductive network between the positive active materials might be inadequate. Some other investigations reported that an increase in the doping nitrogen content could improve the electrical conductivity of carbon-based materials [13–15]. This study also approved that an increase in graphitic-N values could enhance the conductivity of NCNTs samples after N doping.

### 3.3.2. Battery Performance Measurements

Five sets of battery coin cells using the prepared cathode electrodes, as explained in Section 2.3, were fabricated. The fabricated batteries with the different cathode electrodes are labeled as B-CNT, B-NCNT-700, B-NCNT-800, B-NCNT-900, and B-NCNT-1000. The electrochemical performances of the prepared batteries using a Neware battery testing system (CT-4008, Neware China Ltd) were evaluated. The batteries' cycling charge/discharge performances were obtained for the voltage range from 3.0 to 4.3 V at different steady current densities. Generally, two typical voltage platforms appear at around 4.00 and 4.15 V, corresponding to two reversible reaction processes of Li<sup>+</sup> de-insertion/insertion of the LMO crystal [43].

All the battery samples were previously activated within a cycle of charge/discharge process under 0.1 C current density. Figure 7a shows the charge/discharge capacity performance of all batteries under 0.1 C for one cycle. It shows that the highest charge/discharge capacity rates for one cycle were obtained for the B-CNTs, B-NCNT-700, and B-NCNT-800 batteries under the 0.1 C current density. Furthermore, the obtained rate of charge/discharge capacity of B-NCNT-900 and B-NCNT-1000 is lower than that of B-CNTs, indicating the nonuniform distribution of their NCNTs' conductive networks probably causes non-efficient free electrons transportation.

The influence of conductive additives on the reversible capacities of the battery at various cycling rates (0.1–10 C) is shown in Figure 7b. The B-NCNT-700 and B-NCNT-800 samples show nearly consistent reversible capacity when the current density is lower than 1 C ( $\leq 1$  C). The gap in reversible capacities between B-NCNT-700 and B-NCNT-800 becomes greater while increasing the current density. When the current density is raised to 10 C (the highest currents density), B-NCNT-800 can still provide a reversible capacity of 90 mAh g<sup>-1</sup>, which means the doped carbon nanotubes with greater graphitic-N species can improve the charge/discharge performance of batteries. However, the performance of the batteries (B-NCNT-700) decreases significantly at 10 C, which could only provide a reversible capacity of less than 85 mAh g<sup>-1</sup>. The performance of all batteries could be restored when the current density is reduced back to 1 C. Figure S2 and Table S1 show each battery's specific energy and energy efficiency at different cycling rates. The measured energy densities for all cells were above 90% when the current density was lower than 3 C. The B-NCNT-800 maintained a high energy efficiency (80.89% at 10 C) while increasing the current density, confirming the higher electrode conductivity than the other cells [44].

Figure 7c–e shows the cyclic discharge performance of batteries under different current densities (1, 3, and 5 C). All cells' reversible capacities and capacity retentions under 5 C are evaluated and represented in Table 4. The results indicated that the B-NCNT-800 possessed the highest reversible capacities and the greatest cycle stability in higher current densities, which might be attributed to the forming of an efficient conductive network and high conductivity of the S-NCNT-800 slurry. Therefore, the NCNT-800 sample might be a suitable choice for fast-charging technologies.

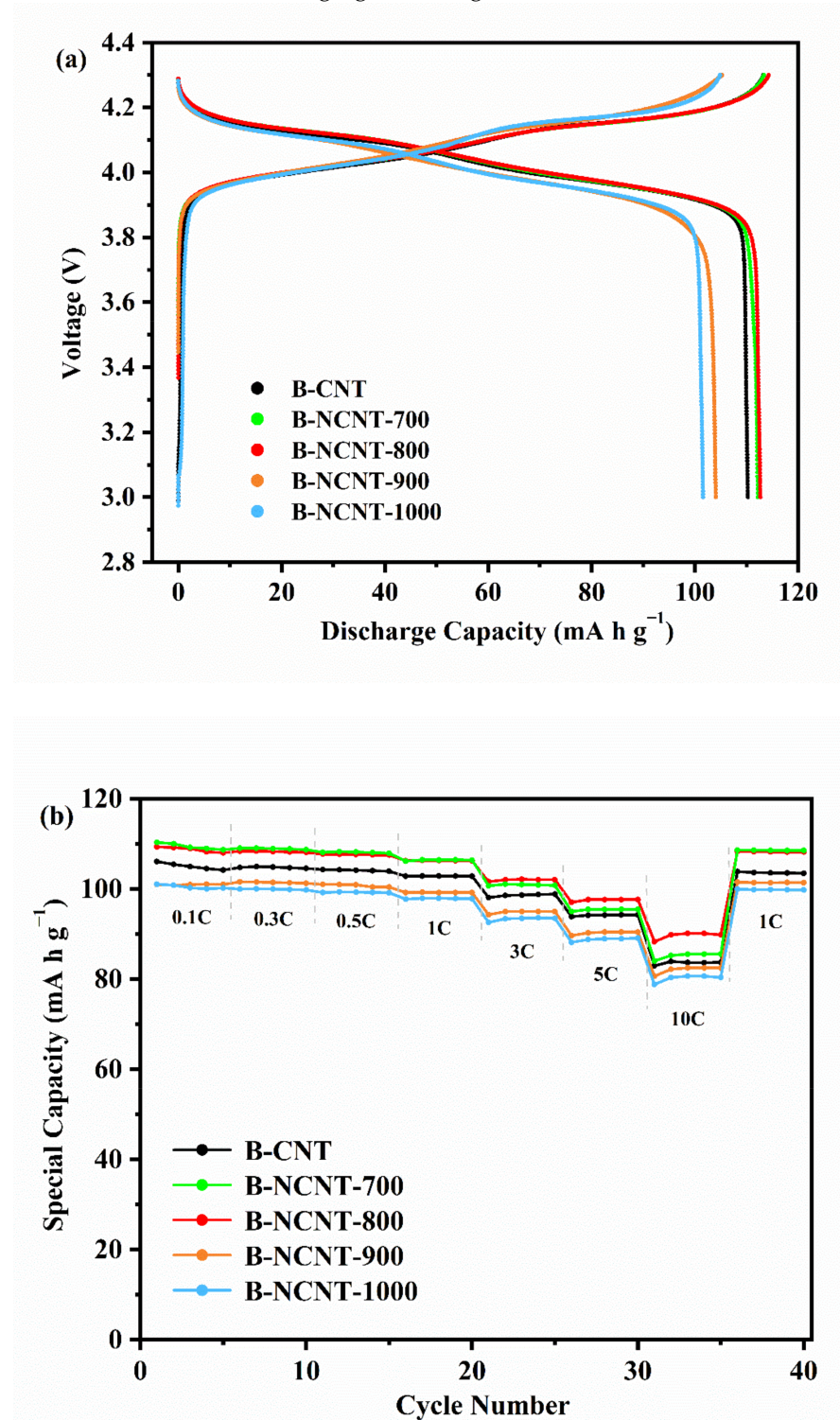


Figure 7. Cont.

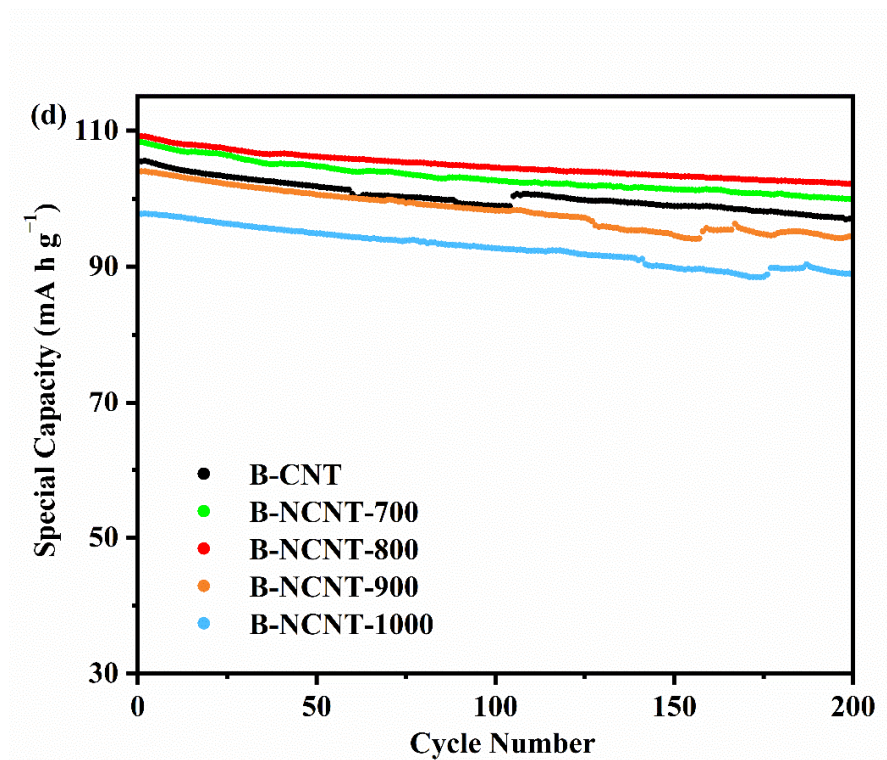
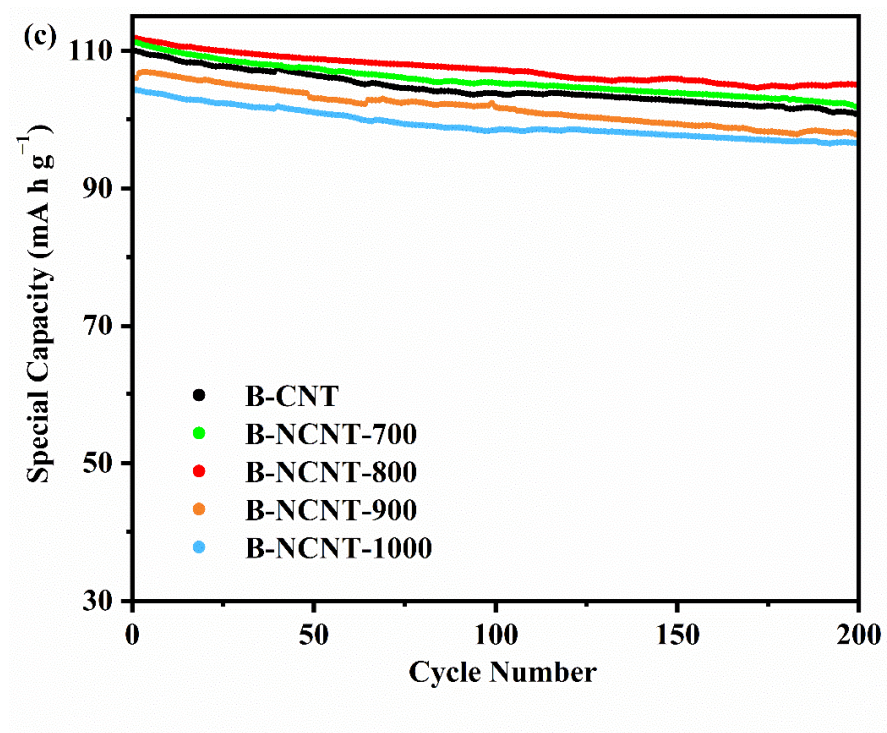


Figure 7. Cont.

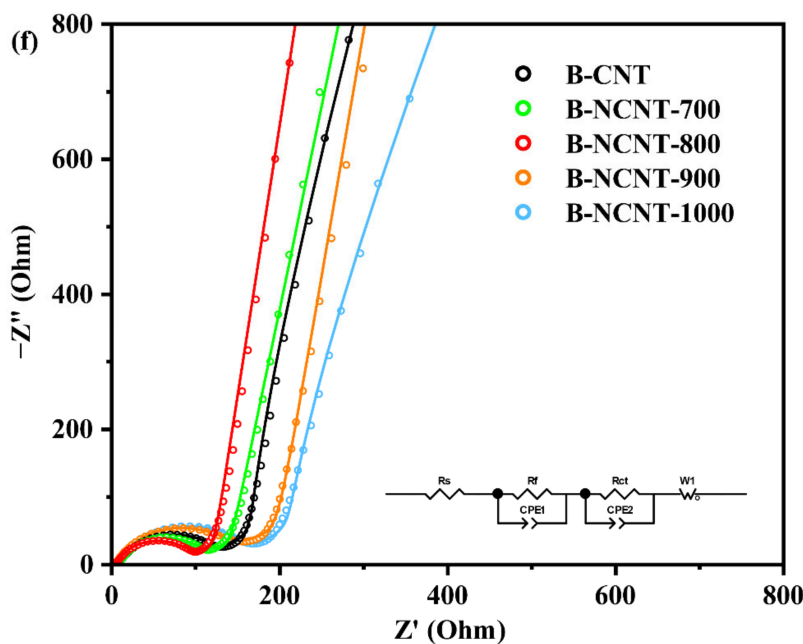
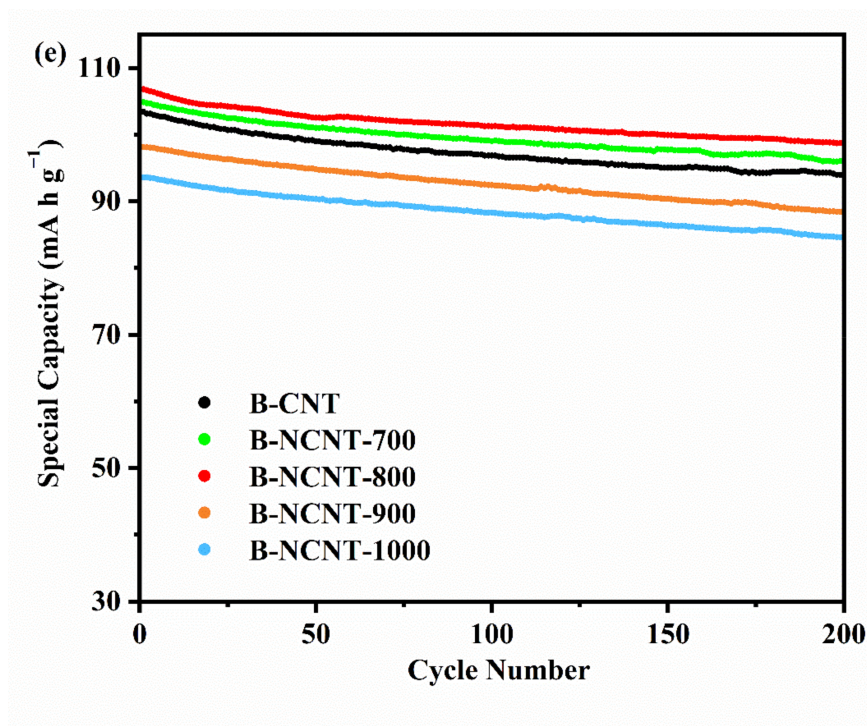


Figure 7. (a–f): Electrochemical performances of lithium-ion batteries. (a) Initial galvanostatic charge/discharge profiles at 0.1 C, (b) rate performance at 0.1–10 C, (c) cycling performance at 1 C, (d) cycling performance at 3 C, (e) cycling performance at 5 C, and (f) Nyquist plot and its fitted curves.

**Table 4.** Battery performance measurements.

Sample	Initial Coulombic Efficiency	Initial Capacity at 5C (mAh g <sup>-1</sup> )	Capacity Retention after 200 Cycles at 5 C	Rct
B-CNT	96.34%	103.44	90.85%	107.7 Ω
B-NCNT-700	97.60%	104.87	91.58%	91.93 Ω
B-NCNT-800	97.30%	106.81	92.45%	81.8 Ω
B-NCNT-900	96.69%	98.13	90.11%	132.6 Ω
B-NCNT-1000	95.48%	93.56	90.45%	141.8 Ω

The impedance spectra (EIS) of the coin cell samples in the frequency ranging from 0.1 to 10<sup>5</sup> Hz with an amplitude of 5 mV were measured by an electrochemical workstation (PGSTAT101, Metrohm Autolab China Ltd). Nyquist plots of coin cells and their equivalent circuit are shown in Figure 7f, where the R<sub>s</sub>, R<sub>ct</sub>, and W represent the resistance of the electrolyte solution, the charge transfer resistance at the particle/electrolyte interface, and the Warburg impedance value, respectively [45]. By fitting the semicircle in the mid-high and high-frequency region, its diameter can reflect the value of the R<sub>ct</sub>. The measured values of R<sub>ct</sub> for all battery samples are represented in Table 4. The measurements revealed that the R<sub>ct</sub> of the B-NCNT-800 is much smaller than other cells. An increase in the electron conductivity of the electrodes decreases the charge-transfer resistance (R<sub>ct</sub>). Higher electron conductivity reduces polarization and improves the battery charge/discharge rate performance, which is reflected in the fitted R<sub>ct</sub> values [46].

The observed oxidation and reduction peaks of the B-NCNT-800 electrode in the CV curve (see Figure S3a) at 4.06 V, 4.18 V (oxidation peaks), and 3.98 V, 4.09 V (reduction peaks) correspond to the reversible de-insertion/insertion process of lithium ions from LiMn<sub>2</sub>O<sub>4</sub> to Li<sub>1-x</sub>Mn<sub>2</sub>O<sub>4</sub>, and then from Li<sub>1-x</sub>Mn<sub>2</sub>O<sub>4</sub> to λ-MnO<sub>2</sub>. The potential interval (ΔV) between the two redox peaks (4.06/3.98 V and 4.18/4.09 V) of B-NCNT-800 was 0.08 and 0.09 V, respectively, which is lower than B-CNT (0.13 and 0.11 V) (see Figure S3b). This phenomenon indicates that using NCNT, as a conductive additive, can reduce the polarization of the electrode [43].

#### 4. Conclusions

A mixture of CNTs and melamine was annealed at different temperatures under argon gas to obtain various samples of NCNT. X-ray Photoelectron Spectroscopical (XPS) measurements showed that the nitrogen doping degree is greater than 5 atom% for the NCNTs sample annealed at 800 °C. The XPS results also approved that the graphitic-N nitrogen groups are the dominating elements obtained on the surface of NCNTs while annealing at 800 °C. The percentage of graphitic-N nitrogen groups decreased while the annealed temperature was lower than 800 °C, which was related to the transformation of pyridinic-N and pyrrolic-N to graphitic-N nitrogen groups needing high temperatures. Besides, the nitrogen content in the prepared NCNT decreased rapidly while the annealing temperature was higher than 800 °C, which was related to the instability of the NCNTs at high temperatures. The doping of graphitic-N elements increased the conductivity of carbon nanotube networks. Compared to the untreated carbon nanotubes (CNTs) sample, the cathode material using the NCNT-800 slurry resulted in a higher rate of initial discharge capability (106.8 mA h g<sup>-1</sup> at 5 C). Moreover, the batteries fabricated by the cathode electrodes using the NCNT-800 slurry showed the best cycling stability performance (92.45% after 200 cycles) for the current density at 5 C. It is hypothesized that the increase in conductive networks by adding the N-doped carbon nanotubes into the coating slurry might increase the proportion of free electrons at the surface of cathode electrodes. We concluded that the addition of conductive networks to cathode material such as the N-doped carbon nanotubes might be a proper method for fast charging applications which still need further investigation.

**Supplementary Materials:** The following supporting information can be downloaded at: <https://www.mdpi.com/article/10.3390/met12122166/s1>, Figure S1: N<sub>2</sub> adsorption/desorption isotherms of CNTs and NCNTs samples. Table S1: Specific energy and energy efficiency of each battery at different cycling rates; title. Figure S2: Energy efficiency of batteries at different cycling rates. Figure S3a–f: CV curves of the B-NCNT-800 (a) and B-CNT (b) cells for second to third cycles at a scan rate of 0.1 mV s<sup>-1</sup> over the potential range of 3.0–4.3 V, the CV curves at diverse scanning rates of the B-NCNT-800 (c) and B-CNT(d), use of eq 1 to analyze the CV data for the B-NCNT-800 and B-CNT(e), and the use of eq 2 to analyze the CV data for the B-NCNT-800 and B-CNT(f).

**Author Contributions:** Conceptualization, Z.Z. and S.Z.; methodology, Z.Z.; software, Z.Z.; validation, Z.Z.; formal analysis, Z.Z.; investigation, Z.Z.; resources, S.Z.; data curation, Z.Z.; writing—original draft preparation, Z.Z.; writing—review and editing, S.M. and D.L.; visualization, Z.Z.; supervision, S.Z.; project administration, S.Z.; funding acquisition, S.Z. All authors have read and agreed to the published version of the manuscript.

**Funding:** This work was supported by the National Natural Science Foundation of China (51874151), the Scientific Research Foundation for Universities from the Education Bureau of Jiangxi Province (GJJ170510), the Natural Science Foundation of Jiangxi Province (20151BBE50106), and the Jiangxi University of Science and Technology (NSFJ2014-G13, Jxxjbs12005).

**Institutional Review Board Statement:** Not applicable.

**Informed Consent Statement:** Not applicable.

**Data Availability Statement:** Not applicable.

**Conflicts of Interest:** The authors declare that they have no competing financial interests or personal relationships that could influence the publication of this research work.

## References

1. Li, L.; Zhang, D.; Deng, J.; Gou, Y.; Fang, J.; Cui, H.; Zhao, Y.; Cao, M. Carbon-based materials for fast charging lithium-ion batteries. *Carbon* **2021**, *183*, 721–734. [[CrossRef](#)]
2. Tomaszewska, A.; Chu, Z.; Feng, X.; O’Kane, S.; Liu, X.; Chen, J.; Ji, C.; Endler, E.; Li, R.; Liu, L. Lithium-ion battery fast charging: A review. *ETransportation* **2019**, *1*, 100011. [[CrossRef](#)]
3. Sehrawat, P.; Julien, C.; Islam, S.S. Carbon nanotubes in Li-ion batteries: A review. *Mater. Sci. Eng. B* **2016**, *213*, 12–40. [[CrossRef](#)]
4. Wei, W.; Guo, L.; Qiu, X.; Qu, P.; Xu, M.; Guo, L. Porous micro-spherical LiFePO<sub>4</sub>/CNT nanocomposite for high-performance Li-ion battery cathode material. *RSC Adv.* **2015**, *5*, 37830–37836. [[CrossRef](#)]
5. Zhang, M.; Ning, G.; Xiao, Z. Binder-Assisted Dispersion of Agglomerated Carbon Nanotubes for Efficiently Establishing Conductive Networks in Cathodes of Li-Ion Batteries. *Energy Technol.* **2020**, *8*, 2000589. [[CrossRef](#)]
6. Luo, W.-b.; Wen, L.; Luo, H.-z.; Song, R.-s.; Zhai, Y.-c.; Liu, C.; Li, F. Carbon nanotube-modified LiFePO<sub>4</sub> for high rate lithium ion batteries. *New Carbon Mater.* **2014**, *29*, 287–294. [[CrossRef](#)]
7. Cruz-Silva, E.; Lopez-Urias, F.; Munoz-Sandoval, E.; Sumpter, B.G.; Terrones, H.; Charlier, J.-C.; Meunier, V.; Terrones, M. Electronic transport and mechanical properties of phosphorus- and phosphorus–nitrogen-doped carbon nanotubes. *ACS Nano* **2009**, *3*, 1913–1921. [[CrossRef](#)]
8. Czerw, R.; Terrones, M.; Charlier, J.C.; Blase, X.; Foley, B.; Kamalakaran, R.; Grobert, N.; Terrones, H.; Tekleab, D.; Ajayan, P.M. Identification of electron donor states in N-doped carbon nanotubes. *Nano Lett.* **2001**, *1*, 457–460. [[CrossRef](#)]
9. Qi, C.; Ma, X.; Ning, G.; Song, X.; Chen, B.; Lan, X.; Li, Y.; Zhang, X.; Gao, J. Aqueous slurry of S-doped carbon nanotubes as conductive additive for lithium ion batteries. *Carbon* **2015**, *92*, 245–253. [[CrossRef](#)]
10. Zhao, L.; Ning, G.; Zhang, S. Green synthesis of S-doped carbon nanotubes via gaseous post-treatment and their application as conductive additive in Li ion batteries. *Carbon* **2021**, *179*, 425–434. [[CrossRef](#)]
11. Cao, Y.; Mao, S.; Li, M.; Chen, Y.; Wang, Y. Metal/porous carbon composites for heterogeneous catalysis: Old catalysts with improved performance promoted by N-doping. *Acs Catal.* **2017**, *7*, 8090–8112. [[CrossRef](#)]
12. Song, X.; Ning, G.; Ma, X.; Yu, Z.; Wang, G. N-doped carbon nanotube-reinforced N-doped mesoporous carbon for flue gas desulfurization. *Ind. Eng. Chem. Res.* **2018**, *57*, 4245–4252. [[CrossRef](#)]
13. Wiggins-Camacho, J.D.; Stevenson, K.J. Effect of nitrogen concentration on capacitance, density of states, electronic conductivity, and morphology of N-doped carbon nanotube electrodes. *J. Phys. Chem. C* **2009**, *113*, 19082–19090. [[CrossRef](#)]
14. Wei, D.; Liu, Y.; Wang, Y.; Zhang, H.; Huang, L.; Yu, G. Synthesis of N-doped graphene by chemical vapor deposition and its electrical properties. *Nano Lett.* **2009**, *9*, 1752–1758. [[CrossRef](#)]
15. Yang, M.; Yang, D.; Chen, H.; Gao, Y.; Li, H. Nitrogen-doped carbon nanotubes as catalysts for the oxygen reduction reaction in alkaline medium. *J. Power Sources* **2015**, *279*, 28–35. [[CrossRef](#)]

16. Idrees, M.; Abbas, S.M.; Ahmad, N.; Mushtaq, M.W.; Naqvi, R.A.; Nam, K.-W.; Muhammad, B.; Iqbal, Z. Mechanistic insights into high lithium storage performance of mesoporous chromium nitride anchored on nitrogen-doped carbon nanotubes. *Chem. Eng. J.* **2017**, *327*, 361–370. [[CrossRef](#)]
17. Lee, W.J.; Maiti, U.N.; Lee, J.M.; Lim, J.; Han, T.H.; Kim, S.O. Nitrogen-doped carbon nanotubes and graphene composite structures for energy and catalytic applications. *Chem. Commun.* **2014**, *50*, 6818–6830. [[CrossRef](#)]
18. Higgins, D.C.; Wu, J.; Li, W.; Chen, Z. Cyanamide derived thin film on carbon nanotubes as metal free oxygen reduction reaction electrocatalyst. *Electrochim. Acta* **2012**, *59*, 8–13. [[CrossRef](#)]
19. Ratso, S.; Kruusenberg, I.; Vikkisk, M.; Joost, U.; Shulga, E.; Kink, I.; Kallio, T.; Tammeveski, K. Highly active nitrogen-doped few-layer graphene/carbon nanotube composite electrocatalyst for oxygen reduction reaction in alkaline media. *Carbon* **2014**, *73*, 361–370. [[CrossRef](#)]
20. Yang, S.; Zhi, L.; Tang, K.; Feng, X.; Maier, J.; Müllen, K. Efficient synthesis of heteroatom (N or S)-doped graphene based on ultrathin graphene oxide-porous silica sheets for oxygen reduction reactions. *Adv. Funct. Mater.* **2012**, *22*, 3634–3640. [[CrossRef](#)]
21. Van Dommele, S.; Romero-Izquierdo, A.; Brydson, R.; De Jong, K.P.; Bitter, J.H. Tuning nitrogen functionalities in catalytically grown nitrogen-containing carbon nanotubes. *Carbon* **2008**, *46*, 138–148. [[CrossRef](#)]
22. Sheng, Z.-H.; Shao, L.; Chen, J.-J.; Bao, W.-J.; Wang, F.-B.; Xia, X.-H. Catalyst-free synthesis of nitrogen-doped graphene via thermal annealing graphite oxide with melamine and its excellent electrocatalysis. *ACS Nano* **2011**, *5*, 4350–4358. [[CrossRef](#)] [[PubMed](#)]
23. Ren, W.; Li, D.; Liu, H.; Mi, R.; Zhang, Y.; Dong, L. Lithium storage performance of carbon nanotubes with different nitrogen contents as anodes in lithium ions batteries. *Electrochim. Acta* **2013**, *105*, 75–82. [[CrossRef](#)]
24. Li, X.; Liu, J.; Zhang, Y.; Li, Y.; Liu, H.; Meng, X.; Yang, J.; Geng, D.; Wang, D.; Li, R.; et al. High concentration nitrogen doped carbon nanotube anodes with superior Li<sup>+</sup> storage performance for lithium rechargeable battery application. *J. Power Sources* **2012**, *197*, 238–245. [[CrossRef](#)]
25. Tian, F.; Nie, W.; Zhong, S.; Liu, X.; Tang, X.; Zhou, M.; Guo, Q.; Hu, S. Highly ordered carbon nanotubes to improve the conductivity of LiNi<sub>0.8</sub>Co<sub>0.15</sub>Al<sub>0.05</sub>O<sub>2</sub> for Li-ion batteries. *J. Mater. Sci.* **2020**, *55*, 12082–12090. [[CrossRef](#)]
26. Tessonnier, J.P.; Su, D.S. Recent progress on the growth mechanism of carbon nanotubes: A review. *ChemSusChem* **2011**, *4*, 824–847. [[CrossRef](#)]
27. Ma, X.; Ji, C.; Liu, Y.; Yu, X.; Xiong, X. Oxygen-rich graphene vertically grown on 3D N-Doped carbon foam for high-performance sodium ion batteries. *J. Power Sources* **2022**, *530*, 231292. [[CrossRef](#)]
28. Yan, S.C.; Li, Z.S.; Zou, Z.G. Photodegradation performance of g-C<sub>3</sub>N<sub>4</sub> fabricated by directly heating melamine. *Langmuir* **2009**, *25*, 10397–10401. [[CrossRef](#)]
29. Zusheng, H.; Linghua, T.; Fayin, J. Non-isothermal kinetic studies on the thermal decomposition of melamine by thermogravimetric analysis. *J. Anal. Sci.* **2011**, *27*, 279.
30. Wu, G.; Mack, N.H.; Gao, W.; Ma, S.; Zhong, R.; Han, J.; Baldwin, J.K.; Zelenay, P. Nitrogen-doped graphene-rich catalysts derived from heteroatom polymers for oxygen reduction in nonaqueous lithium–O<sub>2</sub> battery cathodes. *ACS Nano* **2012**, *6*, 9764–9776. [[CrossRef](#)]
31. Wang, H.; Cote, R.; Faubert, G.; Guay, D.; Dodelet, J.P. Effect of the pre-treatment of carbon black supports on the activity of Fe-based electrocatalysts for the reduction of oxygen. *J. Phys. Chem. B* **1999**, *103*, 2042–2049. [[CrossRef](#)]
32. Kundu, S.; Xia, W.; Busser, W.; Becker, M.; Schmidt, D.A.; Havenith, M.; Muhler, M. The formation of nitrogen-containing functional groups on carbon nanotube surfaces: A quantitative XPS and TPD study. *Phys. Chem. Chem. Phys.* **2010**, *12*, 4351–4359. [[CrossRef](#)]
33. Wang, H.; Maiyalagan, T.; Wang, X. Review on recent progress in nitrogen-doped graphene: Synthesis, characterization, and its potential applications. *AcS Catal.* **2012**, *2*, 781–794. [[CrossRef](#)]
34. Zhang, L.-S.; Liang, X.-Q.; Song, W.-G.; Wu, Z.-Y. Identification of the nitrogen species on N-doped graphene layers and Pt/NG composite catalyst for direct methanol fuel cell. *Phys. Chem. Chem. Phys.* **2010**, *12*, 12055–12059. [[CrossRef](#)]
35. Ning, X.; Li, Y.; Ming, J.; Wang, Q.; Wang, H.; Cao, Y.; Peng, F.; Yang, Y.; Yu, H. Electronic synergism of pyridinic-and graphitic-nitrogen on N-doped carbons for the oxygen reduction reaction. *Chem. Sci.* **2019**, *10*, 1589–1596. [[CrossRef](#)]
36. Pels, J.R.; Kapteijn, F.L.; Moulijn, J.A.; Zhu, Q.; Thomas, K.M. Evolution of nitrogen functionalities in carbonaceous materials during pyrolysis. *Carbon* **1995**, *33*, 1641–1653. [[CrossRef](#)]
37. He, Z.; Dong, B.; Wang, W.; Yang, G.; Cao, Y.; Wang, H.; Yang, Y.; Wang, Q.; Peng, F.; Yu, H. Elucidating interaction between palladium and N-doped carbon nanotubes: Effect of electronic property on activity for nitrobenzene hydrogenation. *ACS Catal.* **2019**, *9*, 2893–2901. [[CrossRef](#)]
38. Kinoshita, K. *Carbon: Electrochemical and Physicochemical Properties*; U.S. Department of Energy, Office of Scientific and Technical Information: Oak Ridge, TN, USA, 1988.
39. Liu, J.; Webster, S.; Carroll, D.L. Temperature and flow rate of NH<sub>3</sub> effects on nitrogen content and doping environments of carbon nanotubes grown by injection CVD method. *J. Phys. Chem. B* **2005**, *109*, 15769–15774. [[CrossRef](#)] [[PubMed](#)]
40. Li, Y.; Mi, R.; Li, S.; Liu, X.; Ren, W.; Liu, H.; Mei, J.; Lau, W.-M. Sulfur–nitrogen doped multi walled carbon nanotubes composite as a cathode material for lithium sulfur batteries. *Int. J. Hydrog. Energy* **2014**, *39*, 16073–16080. [[CrossRef](#)]
41. Li, X.; Wang, H.; Robinson, J.T.; Sanchez, H.; Diankov, G.; Dai, H. Simultaneous nitrogen doping and reduction of graphene oxide. *J. Am. Chem. Soc.* **2009**, *131*, 15939–15944. [[CrossRef](#)] [[PubMed](#)]

42. Jia, X.; Wei, F. Advances in production and applications of carbon nanotubes. In *Single-Walled Carbon Nanotubes*; Springer: Berlin/Heidelberg, Germany, 2019; pp. 299–333.
43. Wang, S.; Luo, C.; Feng, Y.; Fan, G.; Feng, L.; Ren, M.; Liu, B. Electrochemical properties and microstructures of LiMn<sub>2</sub>O<sub>4</sub> cathodes coated with aluminum zirconium coupling agents. *Ceram. Int.* **2020**, *46*, 13003–13013. [[CrossRef](#)]
44. Eftekhari, A. Energy efficiency: A critically important but neglected factor in battery research. *Sustain. Energy Fuels* **2017**, *1*, 2053–2060. [[CrossRef](#)]
45. Chen, X.; Ma, F.; Li, Y.; Liang, J.; Matthews, B.; Sokolowski, J.; Han, J.; Wu, G.; Lu, X.; Li, Q. Nitrogen-doped carbon coated LiNi<sub>0.6</sub>Co<sub>0.2</sub>Mn<sub>0.2</sub>O<sub>2</sub> cathode with enhanced electrochemical performance for Li-Ion batteries. *Electrochim. Acta* **2018**, *284*, 526–533. [[CrossRef](#)]
46. Zhong-Shuai Wu, W.R.; Xu, L.; Li, F.; Cheng, H.-M. Doped Graphene Sheets As Anode Materials with Superhigh Rate and Large Capacity for Lithium Ion Batteries. *ASC Nano* **2011**, *5*, 5463–5471.